Geomechanics and Engineering, *Vol. 22, No. 5 (2020) 449-460*
DOI: https://doi.org/10.12989/gae.2020.22.5.449

A case study on asymmetric deformation mechanism of the reserved roadway under mining influences and its control techniques

Chen Li[1], Zheng Wu[1], Wenlong Zhang[1], Yanhua Sun[3], Chun Zhu*[2] and Xiaohu Zhang[3,4]

[1]*School of Energy & Mining Engineering, China University of Mining and Technology (Beijing), Beijing 100083, China*
[2]*School of Earth Sciences and Engineering, Hohai University, Nanjing, 210098, China*
[3]*School of Civil Engineering, Guizhou University of Engineering Science, Bijie, 551700, China*
[4]*State Key Laboratory for Geomechanics & Deep Underground Engineering, Beijing, 100083, China*

(Received May 25, 2020, Revised July 23, 2020, Accepted August 4, 2020)

Abstract. The double-lane arrangement model is frequently used in underground coal mines because it is beneficial to improve the mining efficiency of the working face. When the double-lane arrangement is used, the service time of the reserved roadway increases by twice, which causes several difficulties for the maintenance of the roadway. Given the severe non-uniform deformation of the reserved roadway in the Buertai Coal Mine, the stress distribution law in the mining area, the failure characteristics of roadway and the control effect of support resistance (SR) were systematically studied through on-site monitoring, FLAC 3D numerical simulation, mechanical model analysis. The research shows that the deformation and failure of the reserved roadway mainly manifested as asymmetrical roof sag and floor heave in the region behind the working face, and the roof dripping phenomenon occurred in the severe roof sag area. After the coal is mined out, the stress adjustment around goaf will happen to some extent. For example, the magnitude, direction, and confining pressure ratio of the principal stress at different positions will change. Under the influence of high-stress rotation, the plastic zone of the weak surrounding rock is expanded asymmetrically, which finally leads to the asymmetric failure of roadway. The existing roadway support has a limited effect on the control of the stress field and plastic zone, i.e., the anchor cable reinforcement cannot fully control the roadway deformation under given conditions. Based on obtained results, using roadway grouting and advanced hydraulic support during the secondary mining of the panel 22205 is proposed to ensure roadway safety. This study provides a reference for the stability control of roadway with similar geological conditions.

Keywords: reserved roadway; asymmetric deformation; stress distribution; plastic zone; surrounding rock control

1. Introduction

The Double-lane arrangement longwall panel system is frequently used in underground coal mines in China. In the longwall panel system, the roadway arrangement in which the haulage roadway of the current longwall panel is excavated simultaneously with the ventilation roadway of adjacent longwall panel is called Double-lane arrangement (Qian *et al.* 2010). One of the two roadways only serves the current longwall panel while the other serves both the current and next adjacent longwall panel. The roadway serving the two panels is called the reserved roadway. Many large collieries adopt double-lane arrangements to alleviate the problems of transportation, ventilation, and replacement tension of panels caused by high mining intensity (Kang *et al.* 2019, Wang *et al.* 2020a). However, the reserved roadway is built to survive the continuously high mining-induced stresses generated by mining the current panel throughout the longwall mining process. Failure of the surrounding rock mass is generally inevitable, which affects the development of engineering (Huang *et al.* 2020, Feng *et al.* 2020). Therefore, large deformation often occurs in the reserved roadway, and the roadway maintenance time is longer, which affects the normal production (Kang *et al.* 2012).

Many scholars have done much research on the stability of roadways. In terms of the stress field of the mining region: Mahdevari *et al.* (Mahdevari *et al.* 2016, Kozłowska *et al.* 2016) systematically studied the evolution of stress field and roadway failure mode during mining based on field monitoring and similar test system. Wang *et al.* (Wang *et al.* 2015, Zhang *et al.* 2019) obtained the vertical stress adjustment range of coal seam on the side of goaf based on the actual measurement. Rezaei *et al.* (Rezaei *et al.* 2015) measured the change of mining-induced stress during the mining of working face by strain energy method. They investigated the failure characteristics and induced fractures of shale. Ma *et al.* (Ma *et al.* 2015, Guo *et al.* 2016) proposed that the variation of principal stress vector in surrounding rocks caused by redistribution of mining dominates the evolution of plastic zone. Kang *et al.* (Kang *et al.* 2017, Shan and Lai *et al.* 2020) studied the far-reaching influence of abnormal residual stress on roadway stability. In terms of deformation and failure mechanism of reserved roadway: Zhao *et al.* (Zhao 2014, Ma *et al.* 2015, Zhao *et al.* 2018, Jia *et al.* 2019) creatively proposed butterfly plastic zone theory under the condition of roadway non-uniform stress field. Liu *et al.* (Liu *et al.* 2017, Wang *et*

*Corresponding author, Lecturer
E-mail: zhuchuncumtb@163.com

ISSN: 2005-307X (Print), 2092-6219 (Online)

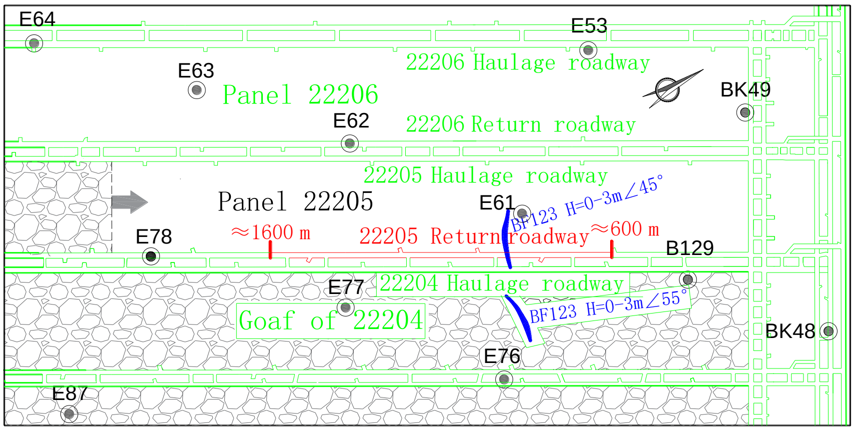

NO.	Depth/m	THK/m	Lithology/E61	Columnar
1	299.3	11.7	Sandy mudstone	
2	311.0	7.8	Fine sandstone	
3	318.8	8.2	Siltstone	
4	327.0	0.9	Clip coal	
5	327.9	4.6	Sandy mudstone	
6	332.5	2.3	2-2 Coal	
7	334.8	0.3	Dirt band	
8	335.1	1.5	2-2 Coal	
9	336.6	3.8	Sandy mudstone	
10	340.4	1.2	Clip coal	
11	341.6	5.1	Sandy mudstone	
12	346.7	6.9	Fine sandstone	

Fig. 1 Mining plan of 2-2 coal seam and column of geological exploration borehole (E61)

al. 2020b) studied the relationship between the failure zone of surrounding rock and principal stress vector in the whole life cycle of mining. Wang *et al.* (2019) studied the distribution and evolution of residual voids in longwall old goaf based on field measurement. Yuan *et al.* (2016) further obtained the roadway failure mechanism by analyzing plastic zone characteristics of deep dynamic pressure roadway. Li *et al.* (2017) obtained the plastic zone distribution pattern of surrounding rock after reserved roadway is affected by primary mining in Hongqingliang Coal Mine through numerical simulation. Jiang *et al.* (2016) obtained the influence of fracture failure on roadway stability by studying the relationship between rock mass fracture and stiffness. Besides, the instability process of surrounding rock caused by underground engineering excavation can be reproduced by indoor model tests (Adach *et al.* 2017, Shi *et al.* 2018, Nam *et al.* 2020, Ren *et al.* 2020, Zhang *et al.* 2020a). In the aspect of roadway surrounding rock control: It was concluded that the residual strength of surrounding rock is dependent on support under low confining pressure (Lin *et al.* 2000, Yang *et al.* 2000). Numerical simulation and similarity tests also verified the control effect of bolt SR on plastic zone size and rock separation (Wang *et al.* 2016, Wang *et al.* 2020c). Engineering practice showed that the support strength adopted in collieries roadway engineering could not completely control the roof sage in soft rock roadway (Jia *et al.* 2016, Li *et al.* 2019). Yao *et al.* (Yao 2011, Coggan *et al.* 2012, Liu *et al.* 2018, Zhang *et al.* 2020b) proposed a targeted roof control scheme by analyzing the instability mechanism of roof water-bearing roadway. More and more scholars optimize roadway support design through numerical simulation analysis. Then the stability of surrounding rock was effectively controlled (Lee and Pietruszczak 2008, Carranza-Torres 2009, Islavath and Deb 2018, Xie *et al.* 2019, Liu *et al.* 2020, Wang *et al.* 2020d).

The Buertai Coal Mine is located in Ordos city of Inner Mongolia autonomous region, China. It is the main production colliery in the Shendong mining area, with an annual output of 20 Mt. During the mining of panel 22204 in Buertai Coal Mine, the local area of 22205 return roadway (reserved roadway) has undergone severe asymmetric deformation, which threatened the standard mining of panel 22205 at the later stage. The previous studies are not sufficient reference for the recognition of the severe asymmetric failure under the influence of heavy mining. The plastic zone is a theoretical tool to analyze the failure of roadway surrounding rock, and it also provides an effective method to study the degree, form, and law of roadway surrounding failure (Hill 1998, Hu *et al.* 2019). Therefore, according to the practical problems encountered in the engineering site, the mechanism of asymmetric deformation of the roadway is studied from the perspectives of mining stress evolution law and plastic zone distribution characteristics. In addition, the stress field of SR and its control effect on the plastic zone were analyzed. Finally, according to the existing technical conditions of the colliery, targeted control measures of surrounding rock stability were proposed to ensure the normal use of the roadway.

2. Case engineering background

2.1 Project overview

The 2-2 coal seam currently being mined in Buertai Coal Mine adopted the double-lane arrangement mode. The width of coal pillars between panels was 20 m, the depth of coal seams was about 330 m, and the average coal thickness was 3.3 m. The roof structure of the 2-2 coal seam was complicated, which contained a dirt band. What's more, the roof was water-rich and fissure developed locally. The size of reserved roadway was 5604 m in length, 5.5 m in width, and 3.5 m in height, respectively, and there was a fault BF123 at 927 m. The mining plane relationship and borehole histogram (E61) are shown in Fig. 1. The rock mass properties lithology of the reserved roadway can be obtained by sorting the data of geological prospecting borehole (E61), as shown in Table 1.

After the mining of panel 22204, the general roof sag and local floor heave occurred at the range of 600-1600 m in reserved roadway. The anchor cable with a diameter of 22 mm and length of 8000 mm had no apparent effect after reinforcement. It then continued to use the anchor cable with a diameter of 28.6 mm to reinforce but still cannot control the roof sag. The original support parameters of the roof were listed below. Six rebar bolts (φ 22 mm×2300 mm)

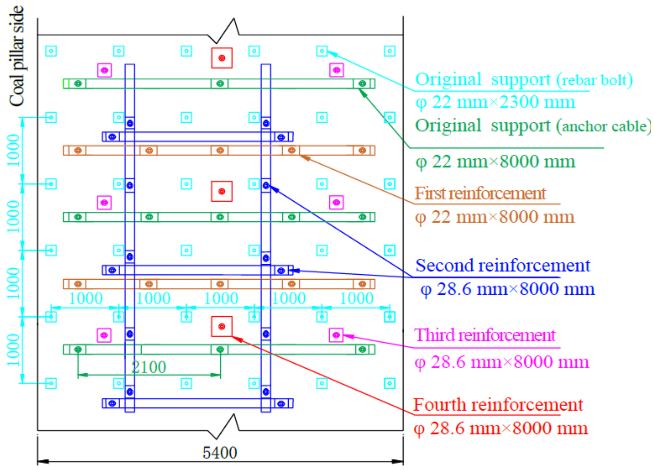

Fig. 2 Roof support plan in severe sag section

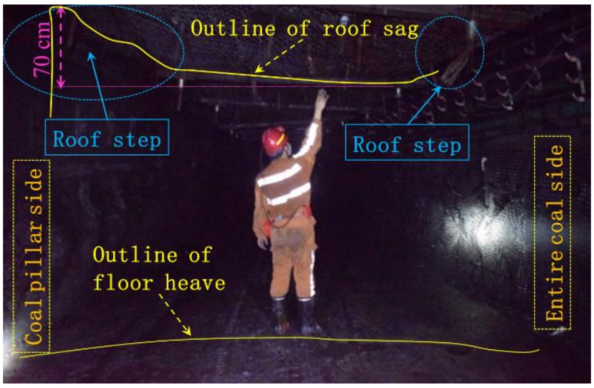

(a) Roof step

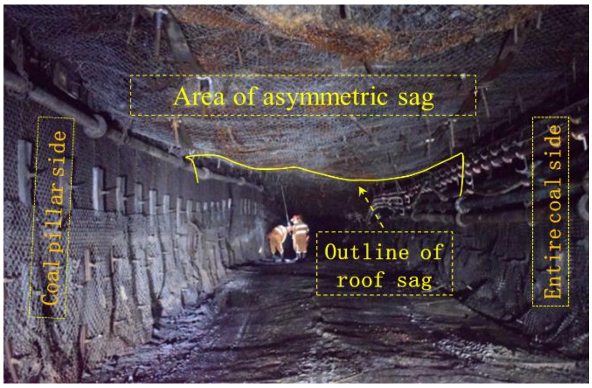

(b) Asymmetric sag

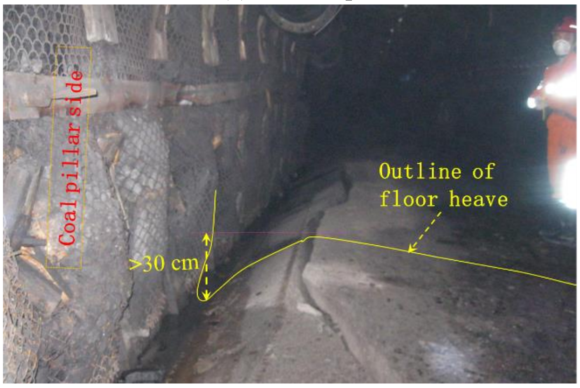

(c) Non-uniform floor heave

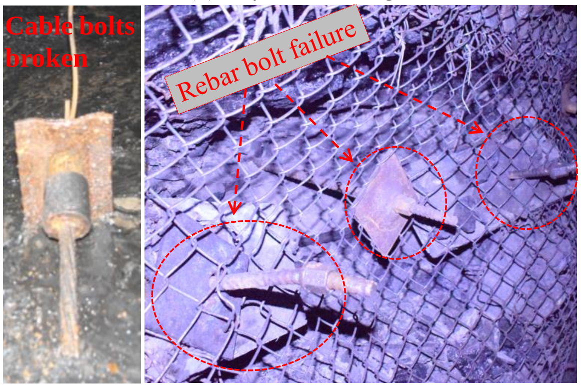

(d) Support failure

Fig. 3 Photos of actual damage at the scene

Table 1 Rock mechanics parameters

Lithology	Tensile strength /MPa	Compressive strength /MPa	Friction angle /°	Cohesion /MPa	Poisson ratio	Softening coefficient
Medium grained sandstone	2.56	45.3	35	8.1	0.21	0.39
Sandy mudstone 5	1.04	32.2	32	5.9	0.19	0.46
Fine-grained sandstone 2	1.37	36.5	29	4.6	0.22	0.33
Sandy mudstone 4	2.07	34.1	35	7.8	0.14	0.35
Siltstone 2	2.07	26.5	34	6.6	0.19	0.47
Sandy mudstone 3	0.62	33.6	29	3.5	0.22	0.23
Clip coal	0.52	9.8	20	1.1	0.21	—

Table 1 Continued

Lithology	Tensile strength /MPa	Compressive strength /MPa	Friction angle /°	Cohesion /MPa	Poisson ratio	Softening coefficient
Siltstone 1	1.66	32.7	29	2.6	0.19	0.27
2-2 coal	0.51	14.1	30	2.9	0.23	—
Sandy mudstone 2	0.62	24.6	29	2.8	0.25	0.26
Clip coal	0.44	7.2	25	1.4	0.14	—
Sandy mudstone 1	1.04	35.4	33	5.2	0.27	0.49
Fine-grained sandstone 1	1.62	38.6	32	6.3	0.22	0.48

were installed on a square pattern of 1000×1000 mm, and three anchor cables (φ 28.6 mm×8000 mm) were installed on the steel belt with 2100 mm spacing and 2000 mm between rows. The original support scheme and reinforcement support scheme under the influence of primary mining in the severe sag section is shown in Fig. 2.

2.2 Profile of roadway failure

Severe intermittent roof sag, rock crush, and floor heave occurred between 650 m and 1650 m of the reserved roadway at the side of the goaf 22204. The roof sag was 400-1100 mm, and the partial roof step was greater than 700 mm, which resulted in the support failure. In addition, the floor heave was greater than 500 mm locally leaded to the floor concrete cracking. The deformation of roadway roof and floor are generally asymmetric, as shown in Fig. 3.

3-point roof separation indicators, as shown in Fig. 4, were installed every 50 m (base points were 2 m, 4 m, and 8 m, respectively) during the drivage of reserved roadway. It can separately show the separation of rock strata in different positions above roof, and timely take effective support measures to ensure safe production (Zhao 2014, Jiang *et al.* 2020). The indicator at severe roof sag area (1500 m) was selected to sort out its historical data, as shown in Fig. 5.

It can be seen from Fig. 5 that the displacement of roof 0-2 m, 2-4 m, and 4-8 m were 352 mm, 282 mm, and 75 mm, respectively. The total movement was 709 mm. The delamination damage in the roof was mainly concentrated within 4 m and accounting for 89%. The failure of deep surrounding rock lagged behind that of shallow rock, and the roadway failure had a visible hysteresis effect. When the monitoring point of the reserved roadway was more than 600 m away from the working face, the roadway tended to be stable.

ZXZ20-Z borehole imager for mining, as shown in Fig. 6, was used to conduct borehole monitoring. The rock character, surrounding rock structure, and fracture development at different locations of the roadway roof can be observed by borehole monitoring. It has significant reference value to roadway support (Jia *et al.* 2019). The full-section monitoring station was drilled at the position of 1250 meters in the reserved roadway, where the roof was water-bearing, and the sag was the largest. The diameter and depth of borehole were 8 mm and 8 m, respectively. The rough results of monitoring are shown in Fig. 7, where the bold red line represents the zone of separation fragmentation, the bold cyan line represents the zone of hole wall roughness and crack development, and the thin black line represents the intact zone.

Fig. 4 The 3-point roof separation indicators

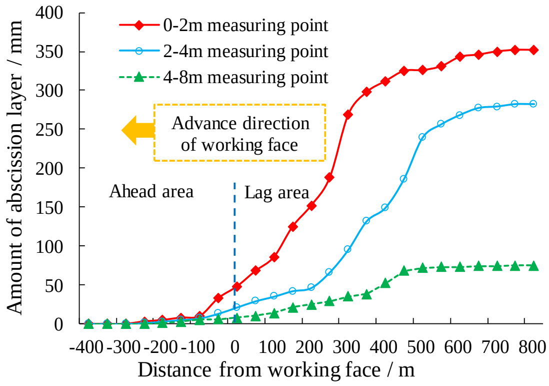

Fig. 5 Curve of roof layer separation at 1500 m

Fig. 6 ZXZ20-Z borehole imager for mining

Fig. 7 shows the results of borehole monitoring. The immediate roof of the roadway was siltstone with a thickness of about 5 m, which contained coal lines and

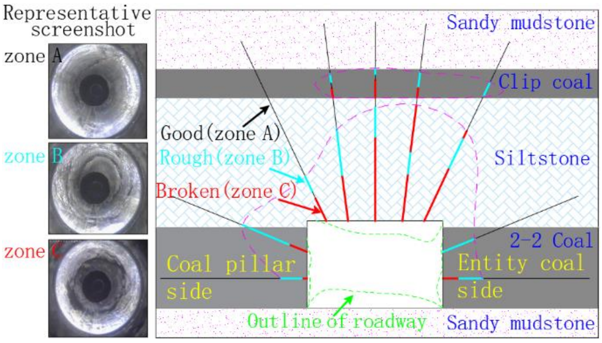

Fig. 7 Borehole monitoring of full-section

small interlayers. The breakaway zone was mainly distributed within 4 m above the roof, and the maximum failure depth appeared in the middle of the roadway. There was clip coal with a thickness of about 1 m above immediate roof, and the inner hole wall of clip coal was rough, the fissure was developed and locally broken. Intact sandy mudstone was above the clip coal. The maximum failure depth of the roadway roof was less than 6 m, and the failure of the roadway rib was less than 2 m. The roadway deformation was asymmetric, and the failure depth measured by borehole monitoring was positively correlated with the roadway surface deformation (Zhao 2014).

3. Analysis of mining-induced stress and plastic failure

In recent years, the application of numerical simulation software has been promoting research and development of engineering (Carranza-Torres 2009, Chen *et al.* 2019, Ren *et al.* 2019, Yokota *et al.* 2019, Choudhary *et al.* 2020). FLAC^{3D} is a numerical simulation software based on the Lagrange difference method, which is mainly used in geotechnical engineering (Giraldo Zapata *et al.* 2018).

To analyze the mining-induced stress distribution law and the plastic failure characteristics of the reserved roadway, a 500×600×200 m (length × width × height) FLAC^{3D} numerical model was established, and the surrounding grid size of roadway was 0.5 m, as shown in Fig. 8. The lateral and bottom boundary of the model was fixed, and the upper boundary was compensated with 5 MPa normal stress. The gravity stress gradient and pressure coefficient in the model were 0.025 and 1.2, respectively. The Mohr-Coulomb constitutive model was adopted in the simulation. Mechanical parameters of coal and rock mass are shown in Table 1.

3.1 Distribution law of mining-induced stress

Panel excavation causes the stress field of the original rock to change dramatically in a certain range. The pressure relief of goaf will lead to different stress superposition in its surrounding area. Therefore, this section will reproduce the stress distribution characteristics under the influence of mining by numerical simulation, which is the basis for studying the mechanism of roadway failure (Wang *et al.* 2018, Wang *et al.* 2020a).

The initial stress balance was carried out in the model, and then the 300 m long working face was pushed forward from 50 m to 450 m. After the stress rebalancing, the distribution data of the mining-induced stress field on the side of goaf was obtained, as shown in Figs. 6-9.

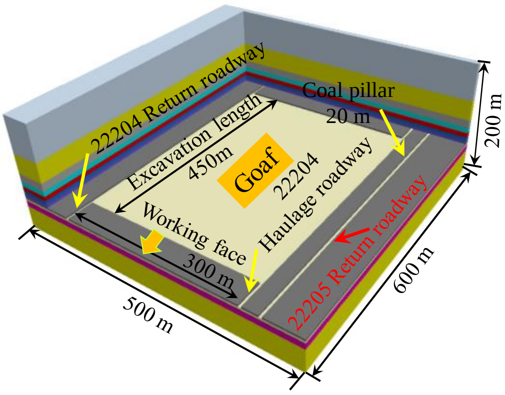

Fig. 8 Model diagram of numerical simulation

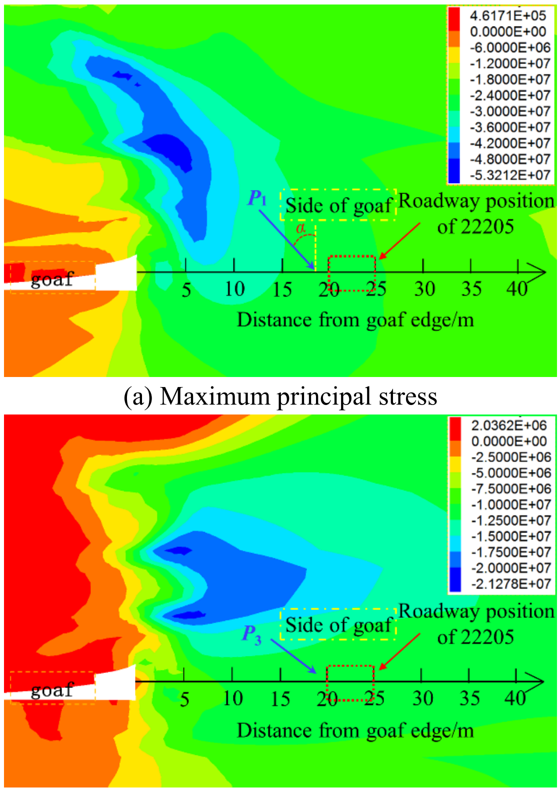

(a) Maximum principal stress

(b) Minimum principal stress

Fig. 9 Distribution of principal stress on the side of goaf

The principal stress concentration phenomenon appeared within the range of 3-15 m away from the side of goaf, and the maximum principal stress (P_1) significantly decreased in the field of 10-20 m. In contrast, the minimum principal stress (P_3) changed little, as shown in Fig. 9. The principal stress on the side of goaf increased sharply from 0-3 m, decreased from 3-6 m, and increased again from 6-9 m. The above phenomenon was because, after water softening, the roof strength was less than coal strength, so that abutment pressure was not transmitted evenly to deep surrounding rock. Then the stress increased and reached its maximum at 9 m away from the goaf. Finally, as the

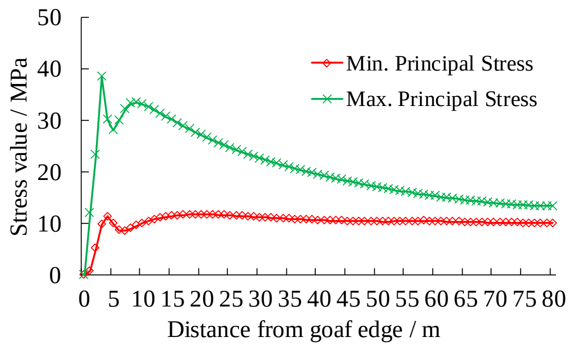

Fig. 10 Principal stress on the side of goaf

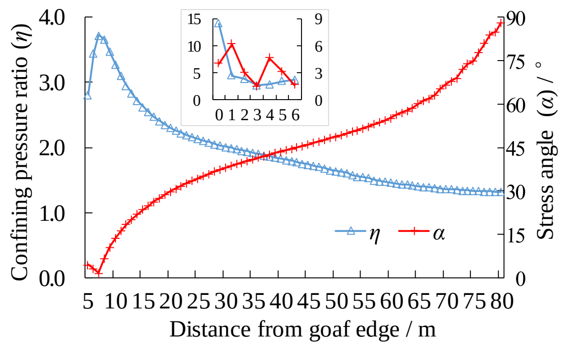

Fig. 11 Confining pressure ratio & stress angle on the side of goaf

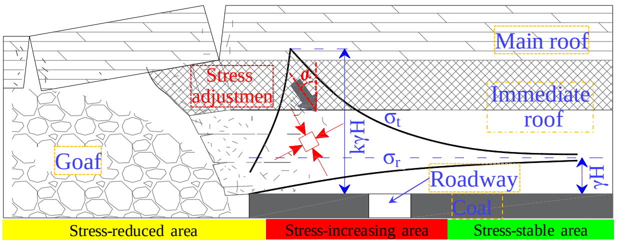

Fig. 12 Stress distribution under mining

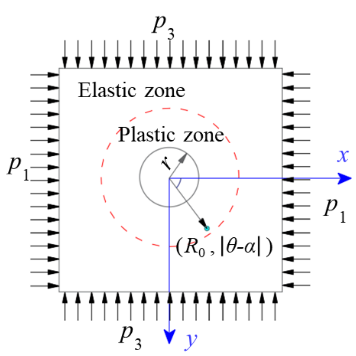

Fig. 13 Mechanical model of the circular roadway

distance from the goaf edge increased, the stress decreased and gradually became stable, as shown in Fig. 10.

The evolution of confining pressure ratio (η, the rate of P_1 to P_3) and stress angle (α, the angle between the P_1 and vertical direction) on the side of goaf are shown in Fig. 11. Within 2 m of goaf margin, the η became very large due to the horizontal stress unloading and the vertical stress concentration. The η gradually decreased within the range of 0-5 m of goaf margin, and then increased to an extreme value of 3.73 at 9 m of goaf margin. Then it decreased with the increase of the distance from goaf, and the reduction became smaller and smaller. The η tended to the coefficient of horizontal pressure eventually. Corresponding to the stress distribution law, the α gradually increased and tended to the original state. For example, the α at 4 m away from goaf was 2°, and the stress deflection was 88° in the numerical model, while the α at 80 m away from goaf was 85° and the stress deflection was only 5°.

3.2 Morphological analysis of plastic zone

Existing research results show that the morphology of the plastic zone is correlated with the deformation of the roadway. The stress environment of the roadway directly determines the morphology of the plastic zone. Therefore, obtaining the shape of plastic zone under different stress conditions has a guiding role for roadway support.

According to the stress distribution, after the coal is mined, the direction and magnitude of the principal stress are adjusted to different degrees with different distances from the goaf (Qian *et al.* 2010), as shown in Fig. 12. Therefore, the stress and α changed dynamically with the change of distance from the goaf.

Ma *et al.* (2015) analyzed the plastic zone boundary of the circular roadway by plane strain calculation based on the Mohr-Coulomb criterion. The mechanical model is shown in Fig. 13. By using the elastic mechanic's theory (Xu 2013), the stress state of a certain point in surrounding rock of circular roadway under the condition of bidirectional non-isobaric pressure is obtained as Eq. (1).

$$\begin{aligned}
\sigma_r &= -\frac{P_1+P_3}{2}\left(1-\frac{r^2}{R_0^{\,2}}\right)+\frac{P_1\text{-}P_3}{2}\cos 2|\theta-\alpha|\left(1-\frac{r^2}{R_0^{\,2}}\right)\left(1-3\frac{r^2}{R_0^{\,2}}\right)\\
\sigma_\theta &= -\frac{P_1+P_3}{2}\left(1+\frac{r^2}{R_0^{\,2}}\right)-\frac{P_1\text{-}P_3}{2}\cos 2|\theta-\alpha|\left(1-3\frac{r^4}{R_0^{\,4}}\right)\\
\tau_{r\theta} &= -\frac{P_1\text{-}P_3}{2}\sin 2|\theta-\alpha|\left(1-\frac{r^2}{R_0^{\,2}}\right)\left(1+3\frac{r^2}{R_0^{\,2}}\right)
\end{aligned} \tag{1}$$

where σ_r, σ_θ and $\tau_{r\theta}$ respectively represent radial stress, circumferential stress and shear stress at any point in the surrounding rock, r is the radius of the roadway, R_0 and θ are the polar coordinates of any position.

The Mohr-coulomb failure criterion in polar coordinates can be expressed by Eq. (2).

$$\begin{aligned}
&\left(\frac{\sigma_r-\sigma_\theta}{2}\right)^2+\tau_{r\theta}-\left(\frac{\sigma_r+\sigma_\theta}{2}\right)^2\sin^2\varphi-\\
&(\sigma_r+\sigma_\theta)\sin\varphi\cos\varphi C-C^2\cos^2\varphi=0
\end{aligned} \tag{2}$$

where φ and C are the internal friction angle and cohesion of rock, respectively.

The mathematical expression of circular roadway plastic zone boundary R_0 under non-isostatic pressure condition can be obtained when the Eq. (1) was substituted into Eq. (2), as Eq. (3).

$$\begin{aligned}
&9(1-\eta)^2\left(\frac{r}{R_0}\right)^8+\left[-12(1-\eta)^2+6(1-\eta)^2\cos 2|\theta-\alpha|\right]\times\left(\frac{r}{R_0}\right)^6+\left[(1-\eta)^2-\sin^2\varphi\left(1+\eta^2+\frac{2C\cos\varphi}{P_3\sin\varphi}\right)^2\right]+\\
&\left[10(1-\eta)^2\cos^2 2|\theta-\alpha|-4(1-\eta)^2\sin^2\varphi\cos^2 2|\theta-\alpha|-2(1-\eta)^2\sin^2 2|\theta-\alpha|-4(1-\eta^2)\cos 2|\theta-\alpha|+(1+\eta)^2\right]\left(\frac{r}{R_0}\right)^4+\\
&\left[-4(1-\eta)^2\cos 4|\theta-\alpha|+2(1-\eta^2)\cos 2|\theta-\alpha|-4(1-\eta^2)\sin^2 2\varphi\cos 2|\theta-\alpha|-\frac{4C(1-\eta)\sin\varphi\cos 2|\theta-\alpha|}{P_3}\right]\left(\frac{r}{R_0}\right)^2=0
\end{aligned} \tag{3}$$

For the plastic zone boundary of roadway in the heterogeneous layered rock mass, when the stress

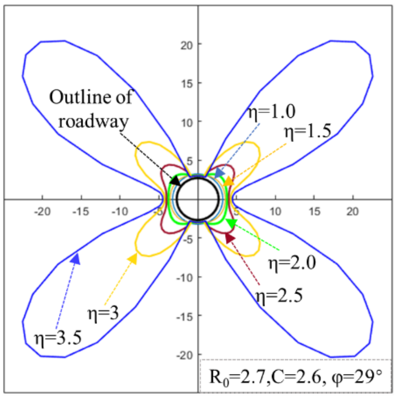

Fig. 14 Relationship between confining pressure ratio and plastic zone of roadway

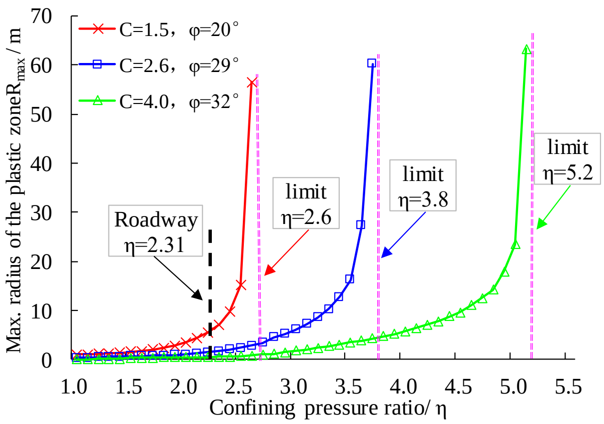

Fig. 15 Stress sensitivity analysis of different surrounding rock lithology

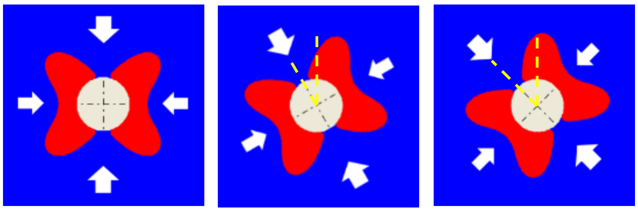

(a) α=0° (b) α=30° (c) α=45°

Fig. 16 Stress sensitivity analysis of different surrounding rock lithology

redistribution of surrounding rock caused by plastic zone expansion deformation is not considered, the mechanical parameters of each stratum are respectively assigned to the Eq. (3), and the plastic zone boundary can be obtained after superposition. MATLAB software was used to calculate the plastic zone boundary under the non-isobaric condition through Eq. (3). The roadway was buried 300 m underground. The relationship between the plastic zone boundary and η is shown in Figs. 14 and 15.

Vertical stress superposition and horizontal stress reduction led to the deflection of principal stress direction and caused the reserved roadway to be in a high η environment. The η controlled the shape of plastic zone. When the η was 1, the plastic zone of roadway was circular. With the increase of η, the roadway plastic zone gradually became elliptic and finally evolved into a butterfly shape.

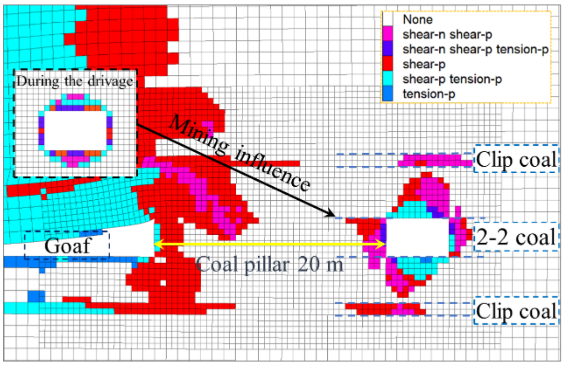

Fig. 17 Plastic zone of roadway

The maximum boundary of the plastic zone was always near the angle bisectors of P_1 and P_3 (Ma *et al.* 2015, Guo *et al.* 2016, Guo *et al.* 2019). Also, the surrounding rocks of different lithologies have different sensitivity to the η function. For example, the η at the location of roadway is 2.31, while the maximum plastic zone of three kinds of rock with different strengths in Fig. 15 is 7.17 m, 1.73 m, and 0.58 m, respectively. There is a positive correlation between rock strength and its limit.

After programming the Eq. (3) in VB, the plastic zone shape of the non-isobaric circular roadway obtained by taking α as the only variable is shown in Fig. 16. When the maximum principal stress and minimum principal stress are in the vertical direction and horizontal direction, respectively, the plastic zone of the roadway is distributed symmetrically. At this moment, the radius of the maximum plastic zone is on the angular bisector in the vertical and horizontal directions, as shown in Fig. 16(a). However, when the direction of the maximum principal stress and the minimum principal stress deflected, the morphology of the plastic zone also changed. When the deflected from 30° to 45°, the maximum plastic zone gradually evolved to the roof of the roadway, which caused a huge hidden danger to the roof, as shown in Fig. 16(b) and 16(c). This is why the butterfly plastic zone of the roadway is no longer symmetrically distributed in the vertical direction.

3.3 Characteristics of the plastic zone in mining roadway

Plastic failure modes of the roadway with different service cycles are obtained through numerical simulation, as shown in Fig. 17. It further reveals the mining failure evolution law of roadway under existing geological conditions.

Under the influence of mining, the roadway was in an environment of high deflecting stress field, and the plastic zone of surrounding rock expanded rapidly and evolved from uniform distribution to “butterfly” asymmetric distribution, as shown in Fig. 17. The plastic zone of roof (floor) suddenly increased from 1.5 m to 4.5 m (3.5 m) and expanded along the coal interlayer. It is because rocks with different strengths have different sensitivity to forming a butterfly plastic zone, and the soft rocks around the roadway will preferentially produce the plastic zone. In addition, the expansion of plastic zone in the interlayer will

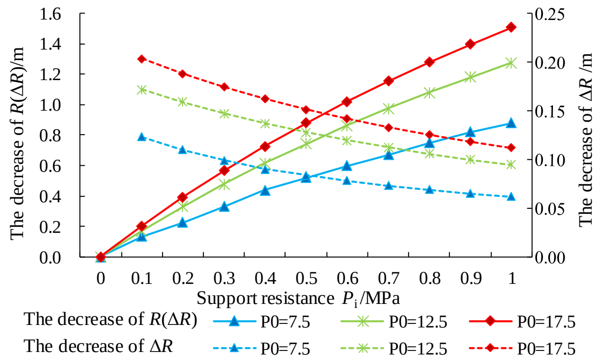

Fig. 18 Sensitivity curve of the plastic zone to SR

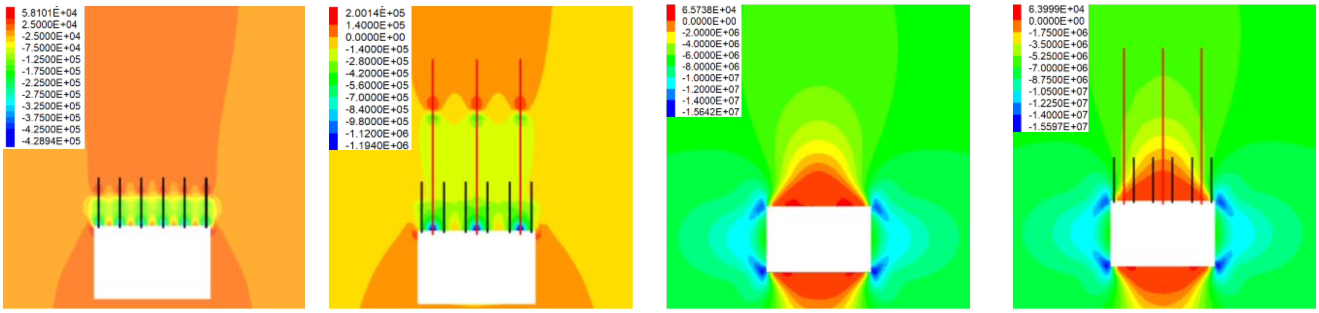

(a) Rebar bolts support (b) Anchor cables support (c) Excavation without support (d) Excavation with support

Fig. 19 Stress field under different conditions

release expansion pressure and act on the roof (floor) in the form of load and further exacerbate roof sag (floor heave) (Zhao *et al.* 2018). The rebar bolts in the roof sag area are completely within the plastic zone, and its supporting function is limited. The plastic zone size is positively related to the deformation (Zhao 2014) so that the sizeable deformation caused by the large plastic zone will result in the anchor cable pulling off or breaking.

4. Analysis of SR control effect on surrounding rock

4.1 Theoretical calculation

Rock mechanics have given the plastic zone radius formula of the circular roadway under support condition (Cai 2013), as shown in Eq. (4).

$$R = r\left[\frac{P_0 + C\cot\varphi}{P_i + C\cot\varphi}(1-\sin\varphi)\right]^{\frac{(1-\sin\varphi)}{2\sin\varphi}} \tag{4}$$

where R is the radius of roadway plastic zone of, r is the roadway radius, P_0 is the original rock stress, P_i is the SR.

The influence of SR on the plastic zone of surrounding rock was analyzed by taking P_i from 0 to 1.0 MPa. The original rock stress P_0 was respectively 7.5 MPa, 12.5 MPa, and 17.5 MPa (corresponding to the buried depth of 300 m, 500 m, and 700 m, respectively). In addition, r, C, and φ were 2.7 m, 3 MPa, and 27°, respectively. It was concluded that the decrease of R (ΔR) increased with the increase of SR, while the decrease of ΔR decreased with each increase of 0.1 MPa. In other words, the sensitivity of support was weaker, as shown in Fig. 18. In the roadway project with a radius of 2.7 m, the SR of 1 MPa is equivalent to at least thirty bolts (the type of φ22 mm) or ten anchor cables (the type of φ22 mm) per meter on the roof, which is far more than the actual situation on the site. That means it is unreasonable to control the plastic zone by intensifying support density (Li *et al.* 2019, Wang *et al.* 2016, Zhao *et al.* 2018).

4.2 Numerical simulation

Cable elements can be used in FLAC^{3D} numerical software to study the stress field distribution characteristics of the support bodies in surrounding rock. A numerical model with a size of 50 m×1 m×50 m was established to study the stress field and plastic zone of support, and the size of grid was 0.2 m. The necessary conditions and parameters were the same as above. The rebar bolts and anchor cables were perpendicular to the roof, and the prestress of rebar bolts and anchor cables, namely the design anchorage force, were 120 kN, and 350 kN respectively with the anchorage length was 1 m and 2 m respectively.

4.2.1 The influence of support on the stress field

The specifications and spacing of the rebar bolts and anchor cables were assigned according to the actual parameter on site. The distribution of support stress field under different conditions is shown in Fig. 19.

Fig. 19 shows the stress field of support and excavation, where (c) and (d) consider the in-situ stress field while (a) and (b) do not. The shallow part of the roof was the compressive stress concentration area under the support effect. In contrast, the anchorage section of the support

Table 2 Form of the support scheme

Support scheme No.	1	2	3	4
No. of rebar bolts		6		
Density of anchor cables (No.·m^{-1})	3	6	9	12
SR (MPa)	0.33	0.52	0.72	0.91

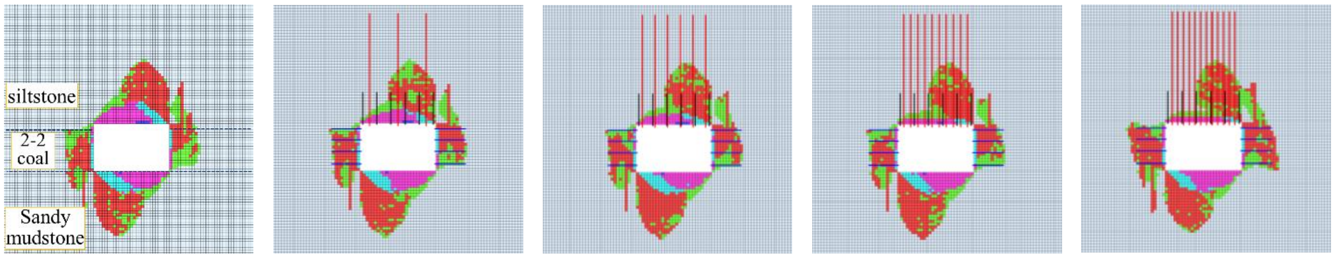

No support Three anchor cables Six anchor cables Nine anchor cables Twelve anchor cables

Fig. 20 Plastic zone at different support density

body formed an obvious tension stress concentration area. When only bolt support was used, the superposition stress in an effective section of the bolt is about 0.15 MPa, while when bolt and cable are used together, the maximum superposition stress in an effective section is about 0.3 MPa, as shown in Fig. 19(a) and 19(b). Fig. 19(c) and 19(d) shows that the P_1 of the regional stress field was 15.642 MPa after roadway excavation under the condition of considering in-situ stress, and it only decreased by 0.045 MPa after support. It can be concluded that the SR is far less than the in-situ stress, and the change of the excavation stress field by support is limited.

4.2.2 The influence of support on plastic zone

The stress at the roadway position in Fig. 9 was assigned to the numerical simulation model. We take the anchor cable with stronger force as the variable, as shown in Table 2, to study the control effect of different support strength on the plastic zone in the roadway roof.

Fig. 20 shows the distribution of the plastic zone under different support density. Under the condition of no support, the plastic zone of roadway surrounding rock presented an asymmetric butterfly distribution, and the maximum failure depth and plastic zone area above the roof were 4.6 m and 16 m^2, respectively. While the support density of roadway roof anchor cables increased from three per meter to twelve per meter, that is, when the SR increased from 0.33 MPa to 0.91 MPa, the maximum depth of plastic zone decreased from 4.6 m to 4.4 m, and the plastic zone area decreased from 14.92 m^2 to 13.28 m^2. In this process, the failure depth only decreases by 0.2 m, and the plastic zone still presents an asymmetric distribution.

For the large deformation roadway of butterfly shape, under the existing support level of roadway engineering, blindly increasing SR has a limited effect on reducing the failure range of surrounding rock (Li *et al.* 2017, Li *et al.* 2019). The essence of support is to anchor the failure rock in the plastic zone to stable rock outside the plastic zone and prevent surrounding rock from instability and falling and control the discontinuous deformation (Zhao *et al.* 2018, Wang *et al.* 2020c). That is to say, the support concept of the mining roadway should change from controlling deformation to controlling roof fall.

5. The mechanism and control of deformation

5.1 Mechanism of asymmetrical deformation

According to the above research results, we can obtain the occurrence mechanism of asymmetric failure of the reserved roadway, as described below.

(1) The strength of the surrounding rock is softened. The geological conditions of the sag section are complicated, faults are developed, and the roof is generally water-rich. Therefore, the strength and cohesion energy of surrounding rock decrease, and the expansion effect is strong, which lead to the decline in rock stability and integrity, and the anchorage of the support body is weakened (Yao 2011, Yin *et al.* 2017, Zhang *et al.* 2020b).

(2) The mechanical environment is complicated. The reserved roadway is in an extremely complex superimposed stress field composed of original rock stress, abutment pressure, dynamic mining load, and expansion pressure in the plastic zone. Besides, the surrounding stress adjustment of goaf causes the principal stress direction to deflect, and the roadway is in the asymmetrical stress field.

(3) The butterfly expansion effect of the plastic zone. The size of the butterfly plastic zone is determined by the η, principal stress, and surrounding rock lithology, which belong to a given quantitative. The sensitivity of different lithology to the η is also different. Therefore, the roadway plastic zone expands in different strata and releases strong deformation pressure, which intensifies roadway failure.

(4) Roadway support is unreasonable. The shallow rock mass above the roof plastic zone will swell with strong expansion pressure and lead to roof sag. Therefore, the elongation of cables cannot match roof deformation and then break. In the later stage, although the large-diameter anchor cable is reinforced, the designed anchorage force is insufficient, so that anchor cables have been pulled out before it is fully extended and the actual supporting effect is limited.

Fig. 21 Advance hydraulic support

5.2 Surrounding rock stability control technology

The reserved roadway was affected by primary mining when panel 22204 was mining, and the roof deformation could not be adequately controlled after the anchor cables reinforcement. The extraction of panel 22205 will make this roadway affected by secondary mining, and the superposition of advanced abutment pressure will inevitably lead to the roadway's violent instability.

Given the above analysis, polymer grouting and shelving support were conducted in severe deformation areas. Grouting holes were constructed in the middle of the roadway with a spacing of 5 m, depth of 5 m, and grouting of 0.5 t marithan per hole. Five ZQL2×22500/22/40d advanced hydraulic supports were arranged in the roadway within 40 m ahead of the working face, as shown in Fig. 21, to prevent roadway roof caving. After taking measures, absolute results had been achieved. Although the anchor cables still broke occasionally when the roadway was affected by secondary mining, it can guarantee the safety of working face to push through the sag section.

5.3 Stability control suggestions for roof sag

In some roadway engineering site, the large deformation of surrounding rock cannot be adequately controlled even if the roadway is reinforced in time (Wang *et al.* 2016). Based on the analysis of SR control effect on surrounding rock above, the following roadway support suggestions were proposed according to the actual situation of large deformation in the reserved roadway of Buertai Coal Mine. For "given deformation" of a large deformation roadway, the idea of stability control should be changed from deformation control to anti-roof disaster. The targeted thinking is as follows. (1) Certain deformations are allowed for relief of pressure. (2) The effective length of anchor cable should be longer than the maximum depth of the plastic zone. (3) Anchor cables bearing capacity should be greater than the weight of the plastic zone. (4) The extension of anchor cables should be greater than the deformation of surrounding rock. (5) The shallow roof should have a certain density of rebar bolts to prevent roof leakage. (6) If the amount of sag is more than 70% of the cable elongation, the cable support should be reinforced in time to provide continuous SR.

6. Conclusions

- When the reserved roadway is affected by primary mining, the roof sag area generally drips water. Rock breakage and separation development within 4 m above the roof is the main concentration area of roof sag. The 5-6 m above the roof is the clip coal, and the cracks are developed. The roadway deformation tends to be stable after 400 m behind the working face.
- The coal seam high-stress concentration range of the P_1 and P_3 on the side of goaf is about 60 m and 15 m, respectively, while the η and α change greatly within the range of 80 m at the side of the goaf. Based on this, the expression and characteristics of the circular roadway plastic zone under non-isobaric conditions are obtained. When the η gradually increases from 1 to a specific value, the shape of the plastic zone will evolve from circle to butterfly shape, and its asymmetric distribution shape is affected by the α.
- Theoretical calculation and numerical analysis show that the sensitivity of the plastic zone to the SR gradually weakens. This paper analyzed the relationship between the SR and the in-situ stress field in engineering practice. It concluded that increasing the SR within a certain range has a limited effect on reducing the failure range of roadway surrounding rock. The support is of considerable significance in preventing the instability and falling of surrounding rock and controlling the discontinuous deformation.
- After mining, the non-symmetric high-stress environment is formed (η=2.3, α=30°), which produces the butterfly plastic zone and causes the deflection of the plastic zone. Finally, it leads to the asymmetric distribution of the plastic zone. The failure of soft clip coal in roof and floor further aggravates roadway deformation. Polymer grouting technology was adopted, and hydraulic support was arranged within 40 m ahead of the working face in the reserved roadway during the secondary mining. The technology of surrounding rock control has obtained a good application effect.

Acknowledgments

This work was supported by the Fundamental Research Funds for the Central Universities (2020YJSNY09), the Research and Development Project of Guizhou University of Engineering Science (Grant No: G2018016), Technology Top Talent Support Project of Guizhou Provincial Education Department ([2017]098), and Technology Platform and Talent Team Plan Project ([2018]5622). The field information from the study site was provided by the Buertai coal mine, owned by Shendong Coal Group Group Co., Ltd.

Conflict of interest

The authors declare no conflict of interest.

References

Adach-Pawelus, K. (2017), "Influence of the roof movement control method on the stability of remnant", *IOP Conf. Ser. Earth Environ. Sci.*, **95**, 42010-42022. https://doi.org/10.1088/1755-1315/95/4/042022.

Cai, M.F. (2013), *Rock Mechanics and Engineering*, Science Press, Beijing, China.

Carranza-Torres, C. (2009), "Analytical and numerical study of the mechanics of rock bolt reinforcement around tunnels in rock masses", *Rock Mech. Rock Eng.*, **42**(2), 175-228. https://doi.org/10.1007/s00603-009-0178-2.

Chen, S.J., Yin, D.W., Jiang, N., Wang, F. and Zhao, Z.H. (2019), "Mechanical properties of oil shale-coal composite samples", *Int. J. Rock Mech. Min. Sci.*, **123**, 104120. https://doi.org/10.1016/j.ijrmms.2019.104120.

Choudhary, A.K., Pandit, B., Babu and G.L.S. (2020), "Three-dimensional analysis of vertical square anchor plate in cohesionless soil", *Geomech. Geoeng.*, **15**(1), 1-9. https://doi.org/10.1080/17486025.2019.1601265.

Coggan, J., Gao, F., Stead, D. and Elmo, D. (2012), "Numerical modelling of the effects of weak immediate roof lithology on coal mine roadway stability", *Int. J. Coal Geol.*, **90**, 100-109. https://doi.org/10.1016/j.coal.2011.11.003.

Feng, G., Kang, Y., Wang, X.C., Hu, Y.Q. and Li, X.H. (2020), "Investigation on the failure characteristics and fracture classification of shale under brazilian test conditions", *Rock Mech. Rock Eng.*, **53**, 3325-3340. https://doi.org/10.1007/s00603-020-02110-6.

Giraldo Zapata, V.M., Botero Jaramillo, E. and Ossa Lopez, A. (2018), "Implementation of a model of elastoviscoplastic consolidation behavior in Flac 3D", *Comput. Geotech.*, **98**, 132-143. https://doi.org/10.1016/j.compgeo.2017.11.011.

Guo, X.F., Ma, N.J., Zhao, X.D. and Zhao, Z.Q. (2016), "General shapes and criterion for surrounding rock mass plastic zone of round roadway", *J. China Coal Soc.*, **41**, 1871-1877. https://doi.org/10.13225/j.cnki.jccs.2016.0787.

Guo, X.F., Zhao, Z.Q., Gao, X., Wu, X.Y. and Ma, N.J. (2019), "Analytical solutions for characteristic radii of circular roadway surrounding rock plastic zone and their application", *Int. J. Min. Sci. Technol.*, **29**(2), 263-272. https://doi.org/10.1016/j.ijmst.2018.10.002.

Hill, R. (1998), *The Mathematical Theory of Plasticity*, Oxford University Press, New York, U.S.A.

Hu, S.C., Tan, Y.L., Zhou, H., Ru, W.K., Ning, J.G., Wang, J., Huang, D.M. and Li, Z. (2020), "Anisotropic modeling of layered rocks incorporating planes of weakness and volumetric stress", *Energy Sci. Eng.*, **8**(3), 789-803. https://doi.org/10.1002/ese3.551.

Huang, H., Babadagli, T., Chen, X., Li, H.Z. and Zhang, Y.M. (2020), "Performance comparison of novel chemical agents for mitigating water-blocking problem in tight gas sandstones", *SPE Reserv. Eval. Eng.*, 1-9. https://doi.org/10.2118/199282-PA.

Islavath, S.R. and Deb. D. (2018), "Stability analysis of underground stope pillars using three dimensional numerical modelling techniques", *Int. J. Min. Miner. Eng.*, **9**(3), 198-215. https://doi.org/10.1504/IJMME.2018.096103.

Jia, H.S., Qiao, A.Z. and Jiang, W.Y. (2016), "Deformation-failure characteristics and supporting method of mining tunnel roof in Buertai mine", *J. Henan Polytech. Univ. Nat. Sci.*, **35**, 338-344. https://doi.org/10.16186/j.cnki.1673-9787.2016.03.008.

Jia, H.S., Wang, L.Y., Fan, K., Peng, B. and Pan, K. (2019), "Control technology of soft rock floor in mining roadway with coal pillar protection: A case study", *Energies*, **12**(15), 3009. https://doi.org/10.3390/en12153009.

Jiang, L.S., Sainoki, A., Mitri, H.S., Ma, N.J. and Liu, H.T. (2016), "Influence of fracture-induced weakening on coal mine gateroad stability", *Int. J. Rock Mech. Min. Sci.*, **88**, 307-317. https://doi.org/10.1016/j.ijrmms.2016.04.017.

Jiang, N., Wang, C.X., Pan, H.Y., Yin, D. and Ma, J. (2020), "Modeling study on the influence of the strip filling mining sequence on mining-induced failure", *Energy Sci. Eng.*, **8**(6), 1-17. https ://doi.org/10.1002/ese3.660.

Kang, H.P., Wu, L., Gao, F.Q., Lv, H.W. and Li, J.Z. (2019), "Field study on the load transfer mechanics associated with longwall coal retreat mining", *Int. J. Rock Mech. Min. Sci.*, **124**, 104-114. https://doi.org/10.1016/j.ijrmms.2019.104141.

Kang, H.P., Yan, L.X. and Guo, X.P. (2012), "Characteristics of surrounding rock deformation and reinforcement technology of retained entry in working face with multi-entry layout", *Chin. J. Rock Mech. Eng.*, **31**, 2022-2036. https://doi.org/10.3969/j.issn.1000-6915.2012.10.007.

Kang, J.Z., Shen, W.L., Bai, J.B., Yan, S. and Wang, X.Y. (2017), "Influence of abnormal stress under a residual bearing coal pillar on the stability of a mine entry", *Int. J. Min. Sci. Technol.*, **27**(6), 945-954. https://doi.org/10.1016/j.ijmst.2017.06.012.

Kozłowska, M., Orlecka-Sikora, B., Rudziński, A., Cielesta, S. and Mutke, G. (2016), "Atypical evolution of seismicity patterns resulting from the coupled natural, human-induced and coseismic stresses in a longwall coal mining environment", *Int. J. Rock Mech. Min. Sci.*, **86**, 5-15. https://doi.org/10.1016/j.ijrmms.2016.03.024.

Lee, Y. and Pietruszczak, S. (2008), "A new numerical procedure for elasto-plastic analysis of a circular opening excavated in a strain-softening rock mass", *Tunn. Undergr. Sp. Tech.*, **23**(5), 588-599. https://doi.org/10.1016/j.tust.2007.11.002.

Li, C., Zhang, W.L., Wang, N. and Hao, C. (2019), "Roof stability control based on plastic zone evolution under mining", *J. Min. Saf. Eng.*, **36**, 753-761. https://doi.org/10.13545/j.cnki.jmse.2019.04.014.

Li, Y.E., Guo, X.F., Ma, J. and Huo, T.H. (2017), "Extension characteristics of the "Butterfly-shaped" plastic zone and stability control of deep mining roadway in Xingdong mine", *J. Min. Sci. Technol.*, **2**(6), 566-575.| https://doi.org/10.19606/j.cnki.jmst.2017.06.007.

Lin, C.D., Lu, S.L. and Shi, Y.W. (2000), "Study on supporting effect of soft roof bolt in coal roadway", *J. China Coal Soc.*, **25**, 482-485. https://doi.org/10.13225/j.cnki.jccs.2000.05.008.

Liu, D.K., Gu, Z.L., Liang, R.X., Su, J.W., Ren, D.Z., Chen, B., Huang, C.Q. and Yang, C. (2020), "Impacts of pore-throat system on fractal characterization of tight sandstones", *Geofluids*, **9**, 1-17. https://doi.org/10.1155/2020/4941501.

Liu, H.T., Wu, X.Y., Hao, Z. and Zhao, X.D. (2017), "Evolution law and stability control of plastic zones of retained entry of working face with double roadways layout", *J. Min. Saf. Eng.*, **32**(4), 689-697. https://doi.org/10.13545/j.cnki.jmse.2017.04.013.

Liu, N.F., Li, N., Li, GF., Zhang, Z.Q. and Mu, Y.H. (2018), "Deformation and collapse mechanisms of water-rich soil tunnels", *Soil Mech. Found. Eng.*, **54**(6), 384-394. https://doi.org/10.1007/s11204-018-9485-5.

Ma, N.J., Li, J. and Zhao, Z.Q. (2015), "Distribution of the deviatoric stress field and plastic zone in circular roadway surrounding rock", *J. China U. Min. Technol.*, **44**(2), 206-213. https://doi.org/10.13247/j.cnki.jcumt.000309.

Mahdevari, S., Shahriar, K., Sharifzadeh, M. and Tannant, D.D. (2016), "Assessment of failure mechanisms in deep longwall faces based on mining-induced seismicity", *Arab. J. Geosci.*, **9**(18), 709. https://doi.org/10.1007/s12517-016-2743-9.

Nam, K., Kim, J., Kwak, D., Rehman, H. and Yoo, H. (2020), "Structure damage estimation due to tunnel excavation based on indoor model test", *Geomech. Eng.*, **21**(2), 95-102. https://doi.org/10.12989/gae.2020.21.2.095.

Qian, M.G., Shi, P.W. and Xu, J.L. (2010), *Mining Pressure and Strata Control*, China University of Mining and Technology Press, Xuzhou, China.

Ren, D.Z., Zhou, D.S., Liu, D.K., Dong, F.J., Ma, S.W. and Huang, H. (2019), "Formation mechanism of the Upper Triassic Yanchang Formation tight sandstone reservoir in Ordos Basin—Take Chang 6 reservoir in Jiyuan oil field as an example", *J. Petrol. Sci. Eng.*, **178**, 497-505. https://doi.org/10.1016/j.petrol.2019.03.021.

Ren, F.Q., Zhu, C. and He, M.C. (2020), "Moment tensor analysis of acoustic emissions for cracking mechanisms during schist strain burst", *Rock Mech. Rock Eng.*, **53**(1), 153-170. https://doi.org/10.1007/s00603-019-01897-3.

Rezaei, M., Hossaini, M.F. and Majdi, A. (2015), "Determination of longwall mining-induced stress using the strain energy method", *Rock Mech. Rock Eng.*, **48**(6), 2421-2433. https://doi. org/10.1007/s00603-014-0704-8.

Shan, P.F. and Lai, X.P. (2020), "An associated evaluation methodology of initial stress level of coal-rock masses in steeply inclined coal seams, Urumchi coal field, China", *Eng. Comput.*, **37**, 2177-2192. https://doi.org/10.1108/EC-07-2019-0325.

Shi, G.C., Yang, X.J., Yu, H.C. and Zhu, C. (2018), "Acoustic emission characteristics of creep fracture evolution in double-fracture fine sandstone under uniaxial compression", *Eng. Fract. Mech.*, **210**, 13-28. https://doi.org/10.1016/j.engfracmech.2018.09.004.

Wang, C.X., Jiang, N., Shen, B.T., Sun, X.Z., Zhang, B.C., Lu, Y. and Li, Y.Y. (2019), "Distribution and evolution of residual voids in longwall old goaf", *Geomech. Eng.*, **19**(2), 105-114. https://doi.org/10.12989/gae.2019.19.2.105.

Wang, C.X., Shen, B.T., Chen, J.T., Tong, W.X., Jiang, Z., Liu, Y. and Li, Y.Y. (2020a), "Compression characteristics of filling gangue and simulation of mining with gangue backfilling: An experimental investigation", *Geomech. Eng.*, **20**(6), 485-495. https://doi.org/10.12989/gae.2020.20.6.485.

Wang, H.Y., Dyskin, A., Dight, P., Pasternak, E. and Hsieh, A. (2018), "Review of unloading tests of dynamic rock failure in compression", *Eng. Fract. Mech.*, **225**, 106289 https://doi.org/10.1016/j.engfracmech.2018.12.022.

Wang, H.Y., Dyskin, A., Pasternak, E. and Dight. P. (2020b), "3D crack growth in biaxial compression: Influence of shape and inclination of initial cracks", *Rock Mech. Rock Eng.*, **53**, 3161-3183. https://doi.org/10.1007/s00603-020-02089-0.

Wang, S.W., Mao, D.B., Pan, J.F. and Chen, X.G. (2015), "Measurement on the whole process of abutment pressure evolution and microseismic activities at the lateral strata of goaf", *J. China Coal Soc.*, **40**(12), 2772-2779. https://doi.org/10.13225/j.cnki.jccs.2015.0080.

Wang, W.J., Dong, E.Y. and Zhao, Z.W. (2020c), "Experimental study on mechanical properties of anchorage body and on anchorage mechanism", *J. China Coal Soc.*, **45**, 82-89. https://doi.org/10.13225/j.cnki.jccs.YG19.1436.

Wang, W.J., Yuan, C., Yu, W.J. and Wu, H. (2016), "Stability control method of surrounding rock in deep roadway with large deformation", *J. China Coal Soc.*, **41**, 2921-2931. https://doi.org/10.13225/j.cnki.jccs.2016.1115.

Wang, X., Yuan, W., Yan, Y.T. and Zhang, X. (2020d), "Scale effect of mechanical properties of jointed rock mass: A numerical study based on particle flow code", *Geomech. Eng.*, **21**(3), 259-268. https://doi.org/10.12989/gae.2020.21.3.259.

Xie, S.R., Pan, H., Zeng, J.C., Wang, E. and Chen, D. (2019), "A case study on control technology of surrounding rock of a large section chamber under a 1200-m deep goaf in Xingdong coal mine, China", *Eng. Fail. Anal.*, **104**, 112-125. https://doi.org/10.1016/j.engfailanal.2019.05.039.

Xu, Z.L. (2013), *Elasticity*, *Higher Education Press*, Beijing, China.

Yang, C., Lu, S.L. and Jiang, Y.D. (2000), "The controlling effect of support resistance on the deformation of surrounding rock with different lithology", *J. China U. Min. Technol.*, **29**, 170-173. https://doi.org/CNKI:SUN:ZGKD.0.2000-02-014.

Yao, Q. (2011), "Researches on strength weakening mechanism and control of water-enriched roof of roadway", Ph.D. Dissertation, China University of Mining and Technology, Xuzhou, China.

Yin, Q., Ma, G.W., Jing, H.W., Wang, H.D., Su, H.J., Wang, Y.C. and Liu, R.C. (2017), "Hydraulic properties of 3D rough-walled fractures during shearing: An experimental study", *J. Hydrol.*, **555**, 169-184. https://doi.org/10.1016/j.jhydrol.2017.10.019.

Yokota, Y., Zhao, Z., Nie, W., Date, K., Iwano, K. and Okada, Y. (2019), "Experimental and numerical study on the interface behaviour between the rock bolt and bond material", *Rock Mech. Rock Eng.*, **52**(3), 869-879. https://doi.org/10.1007/s00603-018-1629-4.

Yuan, Y., Wang, W.J., Yuan, C. and Yu, W.J. (2016), "Large deformation failure mechanism of surrounding rock for gate road under dynamic pressure in deep coal mine", *J. China Coal Soc.*, **41**(12), 2940-2950. https://doi.org/10.13225/j.cnki.jccs.2016.1119.

Zhang, N., Liu, W., Zhang, Y., Shan, P.F. and Shi, X.L. (2020a), "Microscopic pore structure of surrounding rock for underground strategic petroleum reserve (SPR) caverns in bedded rock salt", *Energies*, **13**(7), 1565. https://doi.org/10.3390/en13071565.

Zhang, W.L., Qu, X.C., Li, C., Xu, X, Zhang, S.L., Jin, G.D. and Wang, Y.L. (2019), "Fracture analysis of multi-hard roofs based on microseismic monitoring and control techniques for induced rock burst: A case study", *Arab. J. Geosci.*, **12**(24), 784. https://doi.org/10.1007/s12517-019-4972-1.

Zhang, Y., Cao, S.G., Zhang, N. and Zhao, C.Z. (2020b), "The application of short-wall block backfill mining to preserve surface water resources in northwest China", *J. Clean. Prod.*, **261**, 121232. https://doi.org/10.1016/j.jclepro.2020.121232.

Zhao, Z.Q. (2014), "Mechanism of surrounding rock deformation and failure and control method research in large deformation mining roadway", Ph.D. Dissertation, China University of Mining and Technology (Beijing), Beijing, China.

Zhao, Z.Q., Ma, N.J. and Liu, H.T. (2018), "A butterfly failure theory of rock mass around roadway and its application prospect", *J. China U. Min. Technol.*, **47**, 969-978. https://doi.org/10.13247/j.cnki.jcumt.000922.

CC